Monthly Notices
of the
ROYAL ASTRONOMICAL SOCIETY

MNRAS **507,** L1–L5 (2021)
Advance Access publication 2021 June 01

https://doi.org/10.1093/mnrasl/slab050

IKT 16 aka PSR J0058–7218: discovery of a 22 ms energetic rotation-powered pulsar in the Small Magellanic Cloud

C. Maitra [1★] P. Esposito,[2,3] A. Tiengo [2,3,4] J. Ballet,[5] F. Haberl,[1] S. Dai [6,7] M. D. Filipović[6] and M. Pilia[8]

[1]*Max-Planck-Institut für extraterrestrische Physik, Gießenbachstraße 1, D-85748 Garching, Germany*
[2]*Scuola Universitaria Superiore IUSS Pavia, Palazzo del Broletto, piazza della Vittoria 15, I-27100 Pavia, Italy*
[3]*INAF–Istituto di Astrofisica Spaziale e Fisica Cosmica di Milano, via A. Corti 12, I-20133 Milano, Italy*
[4]*Istituto Nazionale di Fisica Nucleare, Sezione di Pavia, via A. Bassi 6, I-27100 Pavia, Italy*
[5]*AIM, CEA, CNRS, Université Paris-Saclay, Université de Paris, F-91191 Gif sur Yvette, France*
[6]*Western Sydney University, Locked Bag 1797, Penrith, NSW 2751, Australia*
[7]*CSIRO Astronomy and Space Sciences, Australia Telescope National Facility, PO Box 76, Epping, NSW 1710, Australia*
[8]*INAF–Osservatorio Astronomico di Cagliari, Via della Scienza 5, I-09047 Selargius, Italy*

Accepted 2021 May 7. Received 2021 May 7; in original form 2021 February 13

ABSTRACT

We report here on the discovery with *XMM–Newton* of pulsations at 22 ms from the central compact source associated with IKT 16, a supernova remnant in the Small Magellanic Cloud (SMC). The measured spin period and spin period derivative correspond to 21.7661076(2) ms and 2.9(3) $\times$ 10^{-14} s s^{-1}, respectively. Assuming standard spin-down by magnetic dipole radiation, the spin-down power corresponds to 1.1 $\times$ 10^{38} erg s^{-1} implying a Crab-like pulsar. This makes it the most energetic pulsar discovered in the SMC so far and a close analogue of PSR J0537–6910, a Crab-like pulsar in the Large Magellanic Cloud. The characteristic age of the pulsar is 12 kyr. Having for the first time a period measure for this source, we also searched for the signal in archival data collected in radio with the Parkes telescope and in γ-rays with the *Fermi*/LAT, but no evidence for pulsation was found in these energy bands.

Key words: radiation mechanisms: general – ISM: individual objects: IKT 16 – ISM: supernova remnants – Magellanic Clouds – radio continuum: ISM.

1 INTRODUCTION

The Large and the Small Magellanic Clouds (LMC and SMC) are gas-rich irregular galaxies orbiting the Milky Way. The relatively close distance of ∼60 kpc to the SMC and low Galactic foreground absorption ($N_{\rm H} \sim 6 \times 10^{20}$ cm^{-2}) enable the study of its entire X-ray source population down to a luminosity of ∼10^{33} erg s^{-1} (Sturm et al. 2013). The recent star formation activity (∼40 Myr ago), has created an environment where a large number of massive stars are expected, many of which are companions in high-mass X-ray binary (HMXB) systems (Harris & Zaritsky 2004). In tune with this, a large population of HMXBs (predominantly Be X-ray binaries) has been discovered and extensively studied in the SMC. Pulsations have been detected in 63 of these systems, confirming their nature as neutron stars. These Be X-ray binary pulsars are typically a few 10 Myr old and have spin periods ranging from 1 to 2000 s (Haberl & Sturm 2016). On the other hand, of the 'younger' population of isolated neutron stars that constitute the rotation powered pulsars, just a handful in number are known. Only seven such systems have been discovered in the SMC until now from radio surveys (McConnell et al. 1991; Crawford et al. 2001; Manchester et al. 2006; Titus et al. 2019) and their detection may be prone to several selection effects and observational biases (see e.g. Titus et al. 2020).

Ideal sites to search for young rotation powered pulsars are supernova remnant (SNR) – pulsar wind nebula (PWN) composites; Composite SNRs are robust indicators of the presence of a young and energetic pulsar powering the PWN by an outflow of relativistic particles that interact with its natal SNR and the surrounding interstellar medium. Only two such systems are known in the SMC at this date, namely DEM S5 and IKT 16 (Maitra et al. 2015; Alsaberi et al. 2019). IKT 16 is a large X-ray and radio-faint SNR, in which a central source of hard X-ray emission was identified using *XMM–Newton* (van der Heyden, Bleeker & Kaastra 2004). In a detailed analysis using additional *XMM–Newton* observations, Owen et al. (2011) found substantial evidence that the unresolved point source detected at the centre of the SNR is a PWN associated with it. Follow-up observations with *Chandra* resulted in resolving the PWN at the centre of IKT 16, the first such conclusive evidence in the SMC (Maitra et al. 2015). The putative neutron star at the centre of the PWN could be seen as a point source using *Chandra* and was ∼3 times brighter than the soft, symmetric nebula surrounding it. This pointed to the presence of an energetic pulsar dominated by non-thermal emission. We report here the discovery of pulsations from the central source in IKT 16 (PSR J0058−7218 from now), confirming its nature as an energetic rotation powered pulsar. Section 2 presents

★ E-mail: cmaitra@mpe.mpg.de

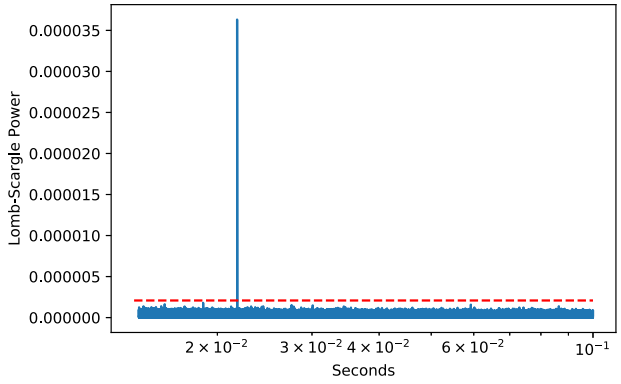

Figure 1. EPIC-pn LSP in the energy band 0.4–10 keV (zoom in). The red dashed line denotes the 3σ confidence levels (taking into account the number of periods searched). The highly significant peak at ∼22 ms reflecting the neutron star rotation is apparent.

the X-ray observations and analysis, Section 3 presents the search for counterparts in the radio and γ-ray wavebands, and the discussion and the conclusions follow in Section 4.

2 OBSERVATION AND ANALYSIS

IKT 16 was observed with the European Photon Imaging Camera (EPIC) onboard the *XMM–Newton* satellite starting on 2020 March 15 for an orbit (Obsid 0841450101). The EPIC-pn (Strüder et al. 2001) was set in small window mode (timing resolution of 5.6718 ms), while both MOS detectors (Turner et al. 2001) were operating in full-frame mode (timing resolution of 2.6 s). All instruments mounted the medium optical-blocking filter. The raw data were analysed with the XMMSAS V.18.00 software package. We searched for periods of high background flaring activity by extracting light curves in the energy range of 7.0–15.0 keV and removed the time intervals with background rates ≥ 8 and 2.5 counts ks^{-1} $arcmin^{-2}$ for EPIC-pn and EPIC-MOS, respectively. Finally, the net exposure times for pn, MOS1, MOS2 are 117.8, 124.4, and 125.9 ks, respectively, not correcting for instrument deadtime. The source counts were selected from a circular region with a radius of 20 arcsec. For the EPIC-pn camera, the background spectra were accumulated in nearby regions in the same CCD as the source, avoiding as much as possible the SNR. The total source and background counts for the PN camera are 6546 and 3868 respectively. In the case of the EPIC-MOS cameras, which were in full-frame mode, background regions were extracted taking into account the SNR centre and size as measured in Owen et al. (2011), so to avoid the SNR emission.

2.1 X-ray timing analysis

To search for a periodic signal, we started with the barycentre-corrected *XMM–Newton* EPIC-pn data (owing to their better time resolution with respect to the MOS data) in the energy range of 0.4–10.0 keV by using a Lomb–Scargle periodogram analysis[1] (LSP) in the period range of 12 ms to 1 s (Lomb 1976; Scargle 1982). A strong periodic signal is detected around 22 ms (Fig. 1). We also verified the result by producing a power-density spectra and found a strong peak at the same frequency. The Fourier power with Leahy normalization (Leahy et al. 1983) corresponded to 592.7 which leads to a chance probability of 3×10^{-122} considering 16777216 trial frequencies searched. A similar exercise performed by extracting events from a large background region did not produce the same peak, thus firmly establishing its origin from the source.

[1] https://docs.astropy.org/en/stable/api/astropy.timeseries.LombScargle.html

Table 1. Spin ephemeris of PSR J0058–7218. We also give for convenience the corresponding period P and period derivative $\dot{P}$, as well as the derived characteristic age $\tau_c = P/(2\dot{P})$, dipolar magnetic field $B \approx (3c^3 I P \dot{P}/(8\pi^2 R^6))^{1/2}$, and rotational energy loss $\dot{E} = 4\pi^2 I \dot{P} P^{-3}$ (here we took $R = 10$ km and $I = 10^{45}$ g cm^2 for the star radius and moment of inertia, respectively). Figures in parentheses represent the 1σ uncertainties in the least significant digit.

Parameter	Value
Range (MJD)	58924.016–58925.583
Epoch (MJD)	58924.0
Frequency, ν (Hz)	45.9429870(4)
Frequency derivative, $\dot{\nu}$ (Hz s^{-1})	$-6.1(6) \times 10^{-11}$
Period, P (ms)	21.7661076(2)
Period derivative, $\dot{P}$ (s s^{-1})	$2.9(3) \times 10^{-14}$
Characteristic age, τ_c, (kyr)	12
Spin down luminosity, $\dot{E}$ (erg s^{-1})	1.1×10^{38}
Surface dipole magnetic field, B_{surf} (G)	8×10^{11}

In order to determine the period more precisely, we employed the Bayesian periodic signal detection method described by Gregory & Loredo (1996). The spin period and its associated 1σ error are determined to 21.7661095(1) ms (without taking into account a period derivative) indicating the spin period of the neutron star in the centre of IKT 16 .

To check for a period derivative, we divided the exposure in nine segments and performed a phase-fitting analysis (see e.g. Phinney 1992). A constant period (a first-order polynomial function) is clearly incompatible with the data, with a reduced χ^2 (χ^2_ν) of 12.85 for 7 degrees of freedom . The introduction of a period derivative (a second-order polynomial) yields an acceptable fit ($\chi^2_\nu = 1.26$ for 6 degrees of freedom). The best-fitting period derivative is $\dot{P} = 2.9(3) \times 10^{-14}$ s s^{-1}. We give the complete phase-coherent spin ephemeris and the derived pulsar properties in Table 1, and in Fig. 2, we show the epoch folded pulse profiles in different energy bands. The pulse profiles are single peaked in all energy bands and do not show any apparent energy dependence. The pulsed fraction, defined as $(M - m)/(M + m)$, where M is the maximum of the pulse profile and m the minimum, is (73 ± 3) per cent, (68 ± 5) per cent, and (79 ± 5) per cent in the 0.4–10 , 0.4–1.5 , and 1.5–10 keV energy bands, respectively. As explained in the next session, the pulsar X-ray emission is contaminated, mainly in the soft energy band, by its PWN and by the surrounding SNR and, therefore, these values should be interpreted as lower limits to the pulsar intrinsic pulsed fraction.

2.2 X-ray spectral analysis

Due to the small size and non-uniformity of the SNR and PWN associated to PSR J0058–7218, these diffuse components cannot be safely subtracted from the pulsar *XMM–Newton* spectrum selecting a nearby background region. However, since the SNR spectrum is rather different from that of the central point source, we defined a background region away from the SNR shock boundary as defined in Owen et al. (2011), and modelled the central source and the SNR emission components in IKT 16 simultaneously in the spectral fit. Since the EPIC-pn was operated in small window mode, such a background region could be properly defined away from the SNR

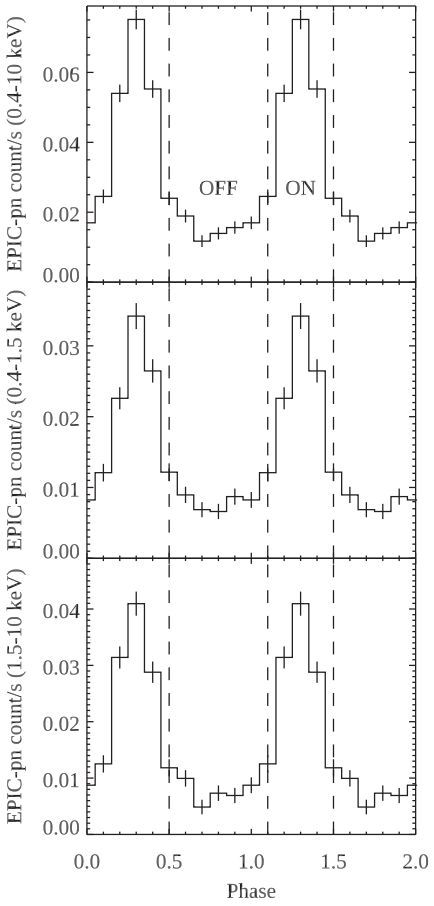

Figure 2. Background-subtracted EPIC-pn light curve folded with the time solution of Table 1 in the 0.4–10 keV (top panel), 0.4–1.5 keV (middle panel), and 1.5–10 keV (bottom panel) energy bands. The dashed vertical lines indicate the on-pulse and off-pulse phase intervals used to study the phase-resolved spectrum.

region only for the MOS cameras. On the other hand, the time resolution of the pn data and the discovery of pulsations allow us to analyse, for the first time, the spectrum of the pulsed emission. In this case, the contribution from both the contaminating sources can be completely eliminated by subtracting the off-pulse emission from the on-pulse spectrum extracted from the same region. The corresponding phase intervals are indicated in Fig. 2.

For the spectral analysis, the XMMSAS tasks `rmfgen` and `arfgen` were used to create the redistribution matrices and ancillary files. Spectra were binned to achieve a minimum of 25 counts per spectral bin. The spectral analysis was performed using the XSPEC fitting package (Arnaud 1996). The X-ray absorption was modelled using the `tbabs` model (Wilms, Allen & McCray 2000) with atomic cross-sections adopted from Verner et al. (1996). We used two absorption components: The first one describes the Galactic foreground absorption, where we used a fixed column density of 6×10^{20} cm^{-2} (Dickey & Lockman 1990) with abundances taken from Wilms, Allen & McCray (2000). The second component accounts for the unknown SMC material in front of the object. For the latter absorption component, the abundances were set to SMC abundances (20 per cent of the solar abundances). We adopted a power-law model to account for the emission from the pulsar. In the MOS phase-averaged spectrum, we included a Sedov component (`vsedov`) to model the SNR emission. The derived $N_{\rm H}$ and SNR parameters are consistent

Table 2. Best-fitting parameters of the phase-averaged (EPIC MOS) and pulsed (EPIC pn) X-ray spectrum of PSR J0058–7218. The line-of-sight Galactic absorption was fixed to 6×10^{20} cm^{-2} and the average spectrum was fitted simultaneously with the SNR emission. Errors are quoted at 90 per cent confidence.

Parameter	Total emission	Pulsed emission[a]
$N_{\rm H}^{\rm local}$ (10^{21} cm^{-2})	4 ± 2	6 ± 2
Γ	1.4 ± 0.1	1.4 ± 0.1
Shock kT (keV)	1.0 ± 0.5	–
Ionization time-scale (10^{11} cm^{-3} s)	1.3 ± 0.5	–
X-ray luminosity[b] (10^{35} erg s^{-1})	1.2 ± 0.1	1.6 ± 0.1
χ^2	100	177
Degrees of freedom	111	156

Note. a Pulsed flux is evaluated with respect to 40 per cent of the duty cycle, see Fig. 2 b Unabsorbed luminosity in the energy band of 0.2–12 keV, assuming a distance of 60 kpc. .

with those obtained in Owen et al. (2011). The power-law index is $\Gamma \sim 1.4$ both in the total and in the pulsed spectrum. Since the PWN emission has a softer spectrum (Maitra et al. 2015), this indicates that, although it cannot be spatially resolved using *XMM–Newton*, its contribution to the total spectrum is marginal. The unabsorbed phase-averaged luminosity of PSR J0058−7218 in the 0.2–12 keV band is $\sim 10^{35}$ erg s^{-1} (see Table 2). The best-fitting parameters of the total and pulsed spectra of PSR J0058−7218 and the errors corresponding to the 90 per cent confidence range are tabulated in Table 2 and the best-fit spectrum is shown in Fig. 3.

3 SEARCH FOR RADIO AND γ-RAY COUNTERPART SOURCES

3.1 Search for a radio counterpart

A 4.5-h long observation pointing at RA = $00^{\rm h}58^{\rm m}06\overset{\rm s}{.}931$, Dec. = $-72^\circ19'17\overset{''}{.}616$, ∼2.1 arcmin from the pulsar, was taken with the Parkes telescope on 2017 August 28 under the project P944 (Titus et al. 2019). The data were recorded at a central frequency of 1382 MHz with a bandwidth of 400 MHz and 1024 frequency channels. The sampling time is 64 μs and only the total intensity was recorded with 2-bit sampling. According to the free electron density model YMW16 (Yao, Manchester & Wang 2017), the dispersion measure (DM) towards the source is expected to be of the order of 140 pc cm^{-3}. Another estimate for DM can be derived by the X-ray absorption column density, $N_{\rm H}$, assuming an ionization fraction. In the Milky Way, the average ionization is ∼10 per cent, as determined empirically from X-ray and radio measurements (He, Ng & Kaspi 2013). The relation is not calibrated for the Magellanic Clouds, but if we assume 10 per cent, the expected DM is consistently ∼150 pc cm^{-3}.

We performed a first targeted search by folding the Parkes data with the position and spin parameters obtained from the X-ray observation. The DSPSR software package (van Straten & Bailes 2011) was used to fold the data with a sub-integration length of 10 s. The PDMP tool as a part of the PSRCHIVE software package (Hotan, van Straten & Manchester 2004) was then used to search through a range of barycentric period and DM (0 – 1000 pc cm^{-3}) to find values giving the highest signal-to-noise ratio for potential pulsar signals. We also carried out a blind search, but no periodic signal was found over a DM range of 0 – 500 pc cm^{-3} using the PRESTO software

package[2] (Ransom 2001; Ransom, Eikenberry & Middleditch 2002). No obvious detection was found in these searches, down to the data set sensitivity of 15 μJy as calculated using the modified radiometer formula for pulsars (Lorimer & Kramer 2004). We also performed a search for single radio pulses using the PYTHON-based pipeline named `SPANDAK`[3] from (Gajjar et al. 2018). Data were first processed through `rfifind` from the PRESTO package for high-level radio frequency interferences purging. The pipeline is based on `Heimdall` (Barsdell et al. 2012) as its main kernel and we used it to search across a DM range from 0 – 1000 pc cm^{-3}. The de-dispersed time series were searched for pulses using a matched-filtering technique with a minimum window size equalling our time resolution (64 μs) and a maximum window size of 65 ms. The pipeline produced around 10 candidates at different DMs. Each candidate found by `Heimdall` was scrutinized to identify possible bursts but none were found down to a limiting fluence of 160 mJy ms.

3.2 Search for a γ-ray counterpart

A young pulsar with such a large $\dot{E}$ is expected to emit strongly in γ-rays and could be visible for *Fermi*/LAT, if the viewing angle is favourable. For example, PSR J0540−6919 in the LMC is easily detected at $2.8 \pm 0.2 \times 10^{-11}$ erg cm^{-2} s^{-1} (0.1–100 GeV). We have looked for a possible γ-ray counterpart in the 4FGL-DR2 catalogue (Abdollahi et al. 2020; Ballet et al. 2020). A faint source (4FGL J0059.7−7210 at $1.6 \pm 0.4 \times 10^{-12}$ erg cm^{-2} s^{-1}) is present 0.18° away from the pulsar's position. The pulsar is just outside the 95 per cent error ellipse of the LAT source, so it could be the counterpart. However, the 4FGL-DR2 catalogue lists the brightest star-forming region in the SMC (NGC 346) as a plausible counterpart. It is closer to the LAT source than the pulsar, so we view the LAT flux as an upper limit to the pulsar's γ-ray flux. The γ-ray spectral shape (curved, peaking just below 1 GeV) can be explained by either a pulsar or a star-forming region.

The LAT photons were folded at the frequency and frequency derivative obtained from the *XMM–Newton* observation, taking the source position from *Chandra*, and no γ-ray pulsation was seen (Smith, private communication). Such a negative result does not make it possible to place a constraining upper limit to the pulsed flux, however, because the LAT source (if it is the pulsar) detects only ∼40 photons per yr, and maintaining phase coherence over 10 yr for a young pulsar requires a more complex ephemeris.

4 DISCUSSION AND CONCLUSIONS

We report the discovery of a young and energetic pulsar PSR J0058–7218 inside the SNR IKT 16 in the SMC. X-ray pulsations are detected corresponding to a period of 21.7661076(2) ms. The pulsar spins down at a rate of $2.9(3) \times 10^{-14}$ s s^{-1} consistent with the scenario expected from a young rotation powered pulsar. Neither radio nor γ-ray pulsations are detected from the existing archival observations using the Parkes and *Fermi*/LAT data respectively. We further extracted the pulsed X-ray emission from PSR J0058–7218 in order to constrain the pulsar's spectral shape and luminosity which is otherwise contaminated by the underlying PWN and SNR emission in the phase averaged spectrum. A photon-index of 1.4

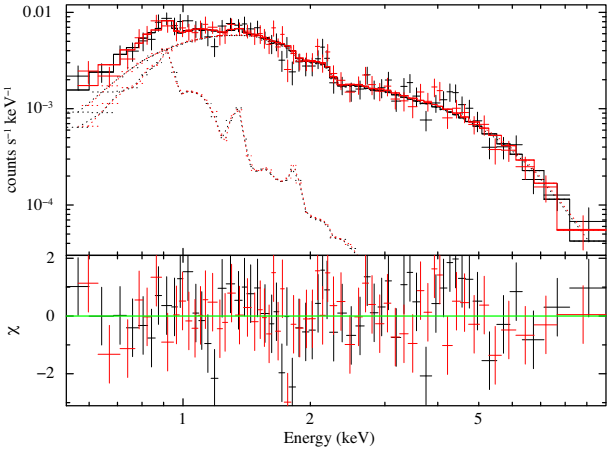

Figure 3. *XMM–Newton* EPIC MOS spectra of PSR J0058–7218 showing MOS1 in black and MOS2 in red. The dotted lines show the contributions of the thermal emission from the SNR (soft) and the power-law emission from the pulsar and the nebula (hard). The residuals for the best-fitting model are shown in the lower panel.

is consistent with that measured typically in other young rotation-powered pulsars where the non-thermal radiation is generated by the particles accelerated in the pulsar magnetosphere (see Becker & Truemper 1997; Wang & Zhao 2004).

The X-ray pulse profile of PSR J0058–7218 is single peaked with a duty-cycle of ≃0.4, and shows no apparent evolution with energy in the range of 0.4–10 keV. The measured spin period and the spin period derivative can be used to derive the spin-down luminosity ($\dot{E}$), characteristic age (τ_c) and the equatorial surface magnetic field ($B_{\rm surf}$) of the pulsar, assuming spin-down by magnetic dipole radiation. The derived parameters of PSR J0058–7218 are given in Table 1. A spin-down luminosity of $\dot{E} \gtrsim 10^{38}$ erg s^{-1} indicates a Crab-like pulsar making it the first such discovery in the SMC and the third in the Magellanic Clouds, the two others being PSR J0537–6910 and PSR J0540–6919 located in the 30 Doradus region of the LMC. A characteristic age of 12 kyr makes it the oldest known Crab-like pulsar. The estimated age is however in line with the Sedov age of 14.7 kyr, derived from the X-ray emission of the SNR (Owen et al. 2011).

Fig. 4 shows the location of PSR J0058–7218 on the P–$\dot{P}$ diagram of pulsars, making it a close analogue of PSR J0537–6910 (the fastest rotating non-recycled pulsar in the LMC SNR N157B; Marshall et al. 1998) in terms of their spin-down properties. The radiation efficiency η_x, which is defined as the ratio of the pulsar's non-thermal X-ray radiation luminosity to the spin-down luminosity (see e.g. Shibata et al. 2016), is also comparable for the two systems, and is of the order of $\sim 10^{-3}$. However, this is about two orders of magnitude smaller than that of the Crab pulsar and PSR J0540−6919. The observed differences (and similarities) in radiation efficiencies can be accounted for by a geometric effect mainly due to differences in the observer's viewing angle (Takata & Cheng 2017). PSR J0537–6910 is also a radio-quiet pulsar, emitting non-thermal X-ray pulsed emission and without detected γ-ray pulsations. This makes it similar to our system at the current detection limits of the radio and γ-ray observations. The above-observed properties could also indicate a geometric effect as the non-detection of radio emission and the thermal X-ray component imply that the polar cap region is hidden from our view. In this case, as the beaming directions of the γ-rays and the non-thermal X-rays may not be the same, our line of sight

[2] https://www.cv.nrao.edu/~sransom/presto/
[3] https://github.com/gajjarv/PulsarSearch

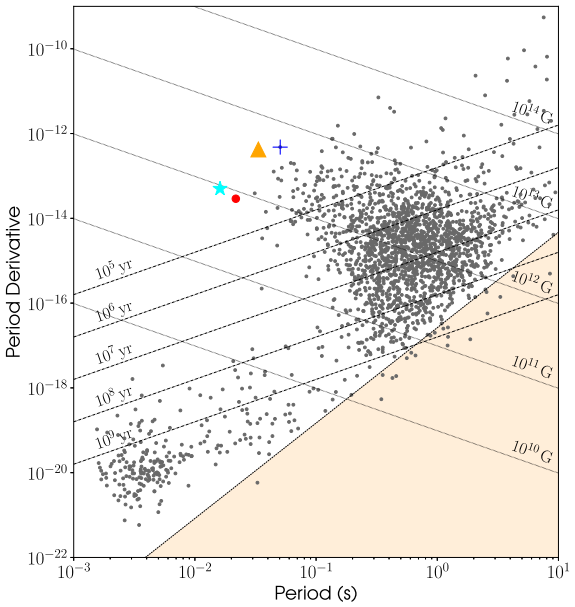

Figure 4. P-Pdot diagram showing the position of PSR J0058–7218 (red dot), PSR J0537–6910 (cyan star), PSR J0540–6919 (orange triangle), and the Crab pulsar (blue cross).

might also miss the γ-ray beam (Cheng, Gil & Zhang 1998; Hui et al. 2017).

The discovery of a young, energetic and ultra-fast pulsar like PSR J0058–7218 provides a unique opportunity to probe the braking mechanisms and birth-spin models of rotation-powered pulsars. Future monitoring of PSR J0058–7218 is crucial to constrain the second derivative of the period in order to measure the braking-index of the pulsar and allow deeper searches in the radio and γ-rays and look for putative glitches that are fairly common in young rotation-powered pulsars on time-scales of a few years. A continuous monitoring of the spin evolution will also be very important because of its potential as a source of detectable gravitational waves (Abbott et al. 2019).

ACKNOWLEDGEMENTS

The authors thank the referee for useful comments and suggestions. This work uses observations obtained with *XMM–Newton*, an ESA science mission with instruments and contributions directly funded by ESA Member States and NASA. The *XMM–Newton* project is supported by the DLR and the Max Planck Society. PE and AT acknowledge funding from PRIN/MIUR award 2017LJ39LM. JB acknowledges support by the Centre National d'Etudes Spatiales (CNES).

DATA AVAILABILITY

X-ray data are available through the High Energy Astrophysics Science Archive Research Center heasarc.gsfc.nasa.gov. The radio data are publicly available from https://data.csiro.au/.C

REFERENCES

Abbott B. P. et al., 2019, ApJ, 879, 10
Abdollahi S. et al., 2020, ApJS, 247, 33
Alsaberi R. Z. E. et al., 2019, MNRAS, 486, 2507
Arnaud K. A., 1996, in Jacoby G. H., Barnes J., eds, ASP Conf. Ser., Vol. 101, Astronomical Data Analysis Software and Systems V. Astron. Soc. Pac., San Francisco,p. 17
Ballet J., Burnett T. H., Digel S. W., Lott B., 2020, preprint (arXiv:2005.11208)
Barsdell B. R., Bailes M., Barnes D. G., Fluke C. J., 2012, MNRAS, 422, 379
Becker W., Truemper J., 1997, A&A, 326, 682
Cheng K. S., Gil J., Zhang L., 1998, ApJ, 493, L35
Crawford F., Kaspi V. M., Manchester R. N., Lyne A. G., Camilo F., D'Amico N., 2001, ApJ, 553, 367
Dickey J. M., Lockman F. J., 1990, ARA&A, 28, 215
Gajjar V. et al., 2018, ApJ, 863, 2
Gregory P. C., Loredo T. J., 1996, ApJ, 473, 1059
Haberl F., Sturm R., 2016, A&A, 586, A81
Harris J., Zaritsky D., 2004, AJ, 127, 1531
He C., Ng C. Y., Kaspi V. M., 2013, ApJ, 768, 64
Hotan A. W., van Straten W., Manchester R. N., 2004, Publ. Astron. Soc. Aust., 21, 302
Hui C. Y., Lee J., Takata J., Ng C. W., Cheng K. S., 2017, ApJ, 834, 120
Leahy D. A., Darbro W., Elsner R. F., Weisskopf M. C., Sutherland P. G., Kahn S., Grindlay J. E., 1983, ApJ, 266, 160
Lomb N. R., 1976, Ap&SS, 39, 447
Lorimer D. R., Kramer M., 2004, Handbook of Pulsar Astronomy, Cambridge Univ. Press, Cambridge
McConnell D., McCulloch P. M., Hamilton P. A., Ables J. G., Hall P. J., Jacka C. E., Hunt A. J., 1991, MNRAS, 249, 654
Maitra C., Ballet J., Filipović M. D., Haberl F., Tiengo A., Grieve K., Roper Q., 2015, A&A, 584, A41
Manchester R. N., Fan G., Lyne A. G., Kaspi V. M., Crawford F., 2006, ApJ, 649, 235
Marshall F. E., Gotthelf E. V., Zhang W., Middleditch J., Wang Q. D., 1998, ApJ, 499, L179
Owen R. A. et al., 2011, A&A, 530, A132
Phinney E. S., 1992, Phil. Trans. R. Soc. A, 341, 39
Ransom S. M., 2001, PhD thesis, Harvard University
Ransom S. M., Eikenberry S. S., Middleditch J., 2002, AJ, 124, 1788
Scargle J. D., 1982, ApJ, 263, 835
Shibata S., Watanabe E., Yatsu Y., Enoto T., Bamba A., 2016, ApJ, 833, 59
Strüder L. et al., 2001, A&A, 365, L18
Sturm R. et al., 2013, A&A, 558, A3
Takata J., Cheng K. S., 2017, ApJ, 834, 4
Titus N. et al., 2019, MNRAS, 487, 4332
Titus N., Toonen S., McBride V. A., Stappers B. W., Buckley D. A. H., Levin L., 2020, MNRAS, 494, 500
Turner M. J. L. et al., 2001, A&A, 365, L27
van der Heyden K. J., Bleeker J. A. M., Kaastra J. S., 2004, A&A, 421, 1031
van Straten W., Bailes M., 2011, Publ. Astron. Soc. Aust., 28, 1
Verner D. A., Ferland G. J., Korista K. T., Yakovlev D. G., 1996, ApJ, 465, 487
Wang W., Zhao Y., 2004, ApJ, 601, 1038
Wilms J., Allen A., McCray R., 2000, ApJ, 542, 914
Yao J. M., Manchester R. N., Wang N., 2017, ApJ, 835, 29

This paper has been typeset from a TEX/LATEX file prepared by the author.